ISSN 1027-5495. Functional Materials, 27, No.2 (2020), p. 378-382.
doi:https://doi.org/10.15407/fm27.02.378

Effects of nickel doping on electronic conductivity and electrochemical properties of $LiMnPO_4/C$

Fengpeng Li, Zhoulan Yin, LiJiao Zhou

School of Chemistry and Chemical Engineering, Central South University, Changsha, 410083 Hunan, China

Received March 2, 2020

Samples of $LiMn_{1-x}Ni_xPO_4/C$ (with x = 0, 0.01, 0.03, 0.05 and 0.1) were synthesized using a combination of spray-drying followed by a traditional ball milling method. XRD analysis shows that the Ni doping does not change the structure of the single $LiMnPO_4$ phase, while SEM studies demonstrated that Ni doping can significantly inhibit aggregation of the synthesized compounds. Electrochemical testing indicates that the Ni doped powders have superior performance relative to the un-doped versions. $LiMn_{0.95}Ni_{0.05}PO_4/C$ has the best electrochemical performance in the measurements of initial capacity and cycling performance. The first specific discharge capacity of this material is 127.4 $mAh{\cdot}g^{-1}$ at a rate of 0.1 C at 25°C, and it retains 88.9 % of its initial capacity after 50 cycles. Improvement of the electrochemical performance of $LiMnPO_4/C$ with Ni doping could be due to improvements in both electrical conductivity and lithium ion diffusion.

Keywords: cathode materials, $LiMnPO_4$, doping, electrical properties, spray-drying.

Образцы $LiMn_{1-x}Ni_xPO_4/C$ (с x = 0; 0,01; 0,03; 0,05 и 0,1) обыли синтезированы с использованием комбинации распылительной сушки с последующим традиционным методом измельчения в шаровой мельнице. Рентгеноструктурный анализ показал, что легирование Ni не меняет структуру отдельной фазы $LiMnPO_4$, в то время как исследования SEM показали, что легирование Ni может значительно ингибировать агрегацию синтезированных соединений. Электрохимические испытания показали, что легированные никелем порошки обладают лучшими характеристиками по сравнению с нелегированными образцами, обладают лучшими электрохимическими характеристиками начальной емкости и циклическими характеристиками. Первая удельная разрядная емкость этого материала составляет 127,4 $мАч{\cdot}г^{-1}$ при скорости 0,1 С при 25°С, и сохраняет 88,9 % своей первоначальной емкости после 50 циклов. Улучшение электрохимических характеристик может быть связана с улучшением как электропроводности, так и с диффузией ионов лития.

Вплив легування нікелем на електронну провідність і електрохімічні властивості $LiMnPO_4$. *Fengpeng Li, Zhoulan Yin, LiJiao Zhou.*

Зразки $LiMn_{1-x}Ni_xPO_4/C$ (з x = 0; 0,01; 0,03; 0,05 та 0,1) интезовано з використанням комбінації розпилювальної сушки з подальшим традиційним методом подрібнення у кульовому млині. Рентгеноструктурний аналіз показав, що легування Ni не змінює структуру окремої фази $LiMnPO_4$, в той час як дослідження SEM показали, що легування Ni може значно пригнічувати агрегацію синтезованих сполук. Електрохімічні випробування свідчать, що леговані нікелем порошки мають кращі характеристики в порівнянні з нелегованої версіями, володіє кращими електрохімічними характеристиками при вимірах початкової ємності і циклічних характеристик. Перша питома розрядна ємність цього матеріалу становить 127,4 $мАг{\cdot}г^{-1}$ при швидкості 0,1 С при 25°С, і він зберігає 88,9 % своєї початкової ємності після 50 циклів. Поліпшення електрохімічних характеристик може бути пов'язано з поліпшенням як електропровідності, так і дифузії іонів літію.

1. Introduction

Lithium-ion batteries have a number of advantages over other energy storage media, so they have become a main candidate for energy storage equipment applications [1]. In the last ten years, $LiCoO_2$ has become the most widely used type [2,3]. However, especially in large-scale applications, this material is relatively expensive, and researchers have been looking for cheap, effective alternatives [4–6]. $LiMPO_4$ (M = Mn, Fe, or Co), a class of transition metal phosphates with an olivine-type structure, has generated significant research interest due to the high chemical and thermal stability of its precursors. Among these, $LiMnPO_4$ is a promising cathode material for current electrolyte systems due to its high capacity (170 $mAh \cdot g^{-1}$) [7]. Unfortunately, because of poor Li^+ insertion/extraction kinetics, the cycling stability and practical capacity of $LiMnPO_4$ is lower than $LiFePO_4$. During the cycling process, both Jahne-Teller lattice deformation and structural changes affect the Li^+ insertion/extraction kinetics [8]. The unacceptable level of capacity attenuation makes it difficult for lithium batteries to make full use of these electrode materials unless they are modified to have better long-term cycling capacity. Several approaches to improve the electrochemical performance of $LiMnPO_4$ have been proposed, including reduction of the Li^+ diffusion length through preparing platelet-like particles, coating the materials with a carbon layer, and metal doping. It was shown that the carbon coating slightly modifies the boundary electron conductivity of $LiMnPO_4$ [9]. Various cations, including Ni^{2+}, Fe^{2+}, Cu^{2+}, Co^{2+}, Ca^{2+}, Zn^{2+}, V^{3+}, Ti^{4+}, Zr^{4+} and their combinations have been studied as dopants in $LiMPO_4$, and cation doping has been shown to be potentially beneficial for performance [10]. The results described in this paper demonstrate that Ni doping, specifically, can improve the performance of $LiMnPO_4$.

In this paper, Ni-doped $LiMnPO_4$/C is first synthesized using a combination of spray-drying followed by ball milling. Compared with other methods, this has an advantage of generating a narrow particle size distribution, and provides a good control of average particle size and composition. Furthermore, the products have high purity and good electrochemical performance. We used $Mn(COOCH_3)_2 \cdot 4H_2O$ as a source of manganese [11], in consideration of both oxidation to Mn^{3+} and dehydration, which ensures that the stoichiometry in the final product is accurate and stable during storage [12]. This precursor exhibits a relatively low decomposition temperature, and the evolved gases (H_2 and CO) additionally pr event further oxidation of manganese(II) ions. The us e of both $Mn(COOCH_3)_2 \cdot 4H_2O$ and $Ni(COOCH_3)_2 \cdot 4H_2O$ salts enables the straightforward synthesis of analogues in the $LiMn_{1-x}Ni_xPO_4$ series [13–15].

2. Experimental

2.1 Sample synthesis

(x = 0, 0.01, 0.03, 0.05 and 0.1) powders were synthesized via a combination of spray-drying followed by ball milling. First, stoichiometric amounts of Li_2CO_3, $NH_4H_2PO_4$, and the desired ratio of $Ni(COOCH_3)_2 \cdot 4H_2O$ and $Mn(COOCH_3)_2 \cdot 4H_2O$ were dissolved in deionized water [16]. With magnetic stirring, this solution was then added to an aqueous solution of citric acid and glucose until a clear product was obtained. In this solution, citric acid acts as a surfactant, and a carbon source [17]. The clear solution was dried at a rate of 20 mL/min using a spray dryer, with the inlet and outlet temperatures maintained at 220°C and 110°C, respectively. The resulting powder was ball-milled at 300 rpm for 4 h, and then held at 350°C for 4 h, followed by holding at 650°C for 12 h in gas shield. The carbon content of the resulting $LiMn_{1-x}Ni_xPO_4$/C is about 15 wt%. Fig. 1 is a flow chart for the synthesis of by the method described here.

Three types of material analysis were performed. XRD (Cu Kα radiation) was used to identify crystalline phases. Morphology of the powders was examined by SEM; the carbon content was determined by C–S analysis, which involves converting all C in the specimen to CO or CO_2, followed by quantification by IR.

The electrochemical properties of the synthesized materials were characterized using a CR2025 coin-type cell. The cathode is composed of 10 wt. % PVDF as a binder, 10 wt. % acetylene black as a conducting agent and 80 wt. % . After blending into NMP, the mixed slurry was dispersed onto aluminum foil and dried in vacuum at 120°C for 12 h. The anode was metallic lithium foil. First, the cell was remained motionless for 6 h after assembly in the glove box, then it was charged and discharged over a voltage range of 2.5–4.6 V (vs. Li/Li^+)

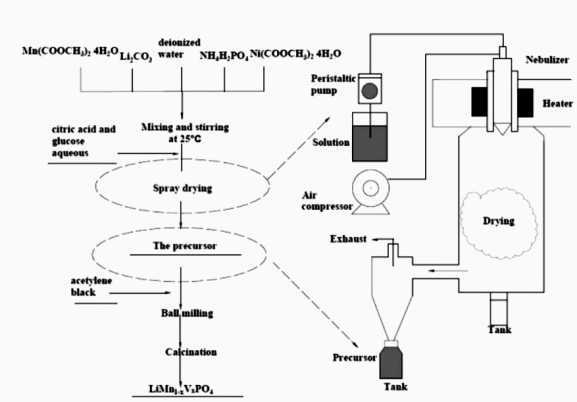

Fig. 1. General flow chart for the synthesis of $LiMn_{1-x}Ni_xPO_4/C$ via spray-drying followed by ball milling.

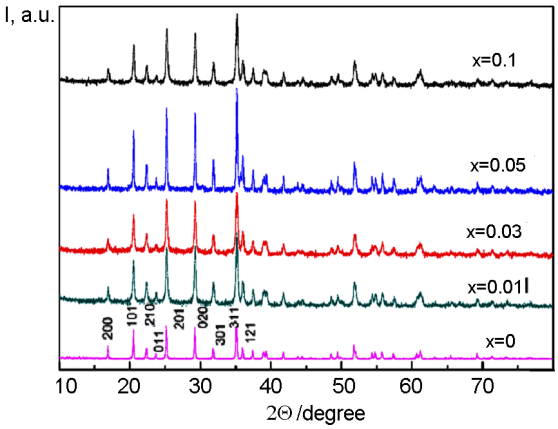

Fig. 2. XRD patterns of $LiMn_{1-x}Ni_xPO_4/C$.

at a 0.1 C. CV curves were recorded in the potential range of 2.5–4.5 V with a scan rate of 0.1 $mV \cdot s^{-1}$ with a CHI660D. EIS spectra were recorded using an AC voltage of 5 mV amplitude in a 0.01 Hz to 100 kHz frequency range.

3. Results and discussion

Fig. 2 shows XRD patterns of the samples. As shown, all diffraction patterns of the samples display a single olivine-type orthorhombic structure in a *Pnmb* space group (JCPDS 74-0375), with no impurity phases. No crystalline carbon (graphite) diffraction peaks appeared, indicating that the carbon obtained from the decomposition of citric acid exists in an amorphous phase. All of the samples have a well-defined crystalline structure, and Ni doping did not change the position of the peaks in the 2θ axis, indicating that the doping had no significant effect on the $LiMnPO_4$ crystal structure. It is found that with an increase in the Ni doping content, the intensities of diffraction peaks decrease. C–S analysis has shown that the carbon contents in the $LiMn_{1-x}Ni_xPO_4/C$ samples are between 4.98 and 5.34 % for x between 0 and 0.1, with no dependence on x.

The SEM image in Fig. 3 shows that all powders exhibit a particle size of 50–200 nm. Compared with the undoped sample, the Ni-doped samples exhibit more uniform particle size and less agglomeration. The Ni doping effectively reduces the aggregation of $LiMnPO_4$. The speed of lithium ion diffusion across the $LiMnPO_4/MnPO_4$ interface can increase with reduced particle size, which would improve the performance properties of

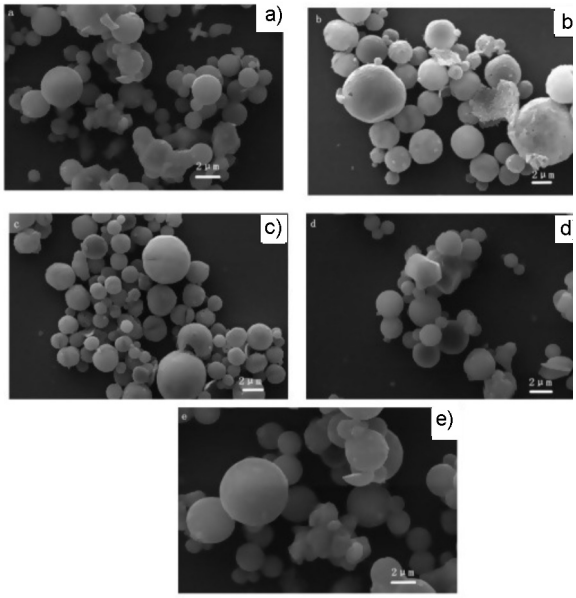

Fig. 3. SEM images of $LiMn_{1-x}Ni_xPO_4/C$ samples. (a) $x = 0$, (b) $x = 0.01$, (c) $x = 0.03$, (d) $x = 0.05$, (e) $x = 0.1$.

$LiMnPO_4$. In addition, the change in morphology becomes smaller with an increase in the amount of Ni dopant. The $LiMn_{0.95}Ni_{0.05}PO_4/C$ sample exhibits the best spherical shape and size of particles, which is advantageous for achieving a high bulk density and energy density. Fig. 4 shows a comparison of the CV curves for $LiMnPO_4/C$ and $LiMn_{0.95}Ni_{0.05}PO_4/C$ samples. For $LiMn_{0.95}Ni_{0.05}PO_4/C$, the reduction and oxidation peak positions are 3.913 V and 4.313 V, respectively ($\Delta E = 0.4$ V), while the peaks for pure $LiMnPO_4/C$ are located at 3.916 V and 4.406 V ($\Delta E = 0.49$ V); so the $LiMn_{0.95}Ni_{0.05}PO_4/C$ sample exhibits a smaller potential difference. The oxidation and reduc-

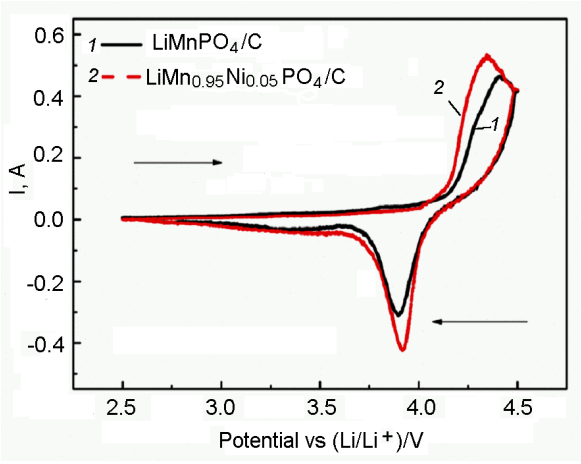

Fig. 4. CV profiles of $LiMnPO_4/C$ and $LiMn_{0.95}Ni_{0.05}PO_4/C$.

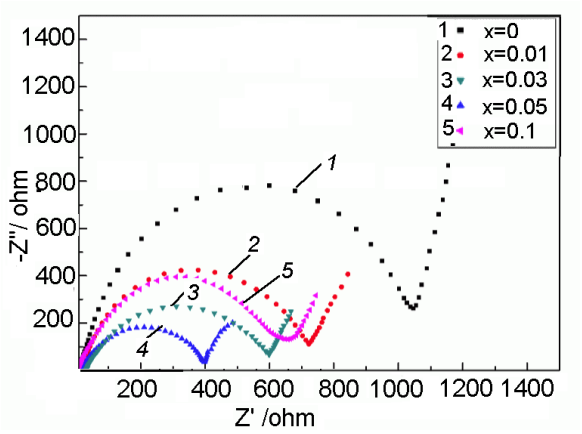

Fig. 5. Nyquist plots of $LiMn_{1-x}Ni_xPO_4/C$.

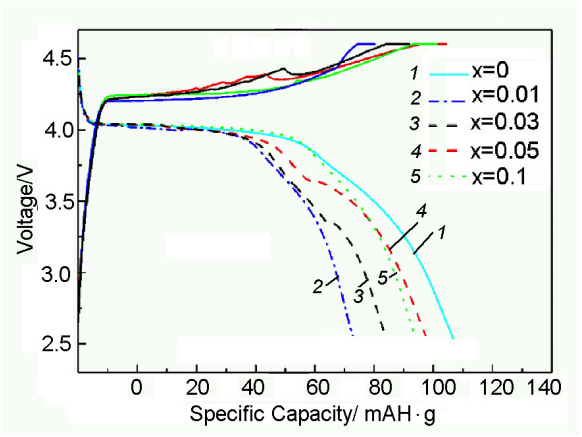

Fig. 6. The initial charge-discharge curves of $LiMn_{1-x}Ni_xPO_4/C$.

tion peaks are related to the reversibility of the electrode reaction. Ni doping reduces the interval, which shows that Ni^{2+} doping can promote the extraction/reinsertion of lithium ions in electrochemical reactions. The Nyquist plots for samples are shown in Fig. 5. The lithium ion diffusion can be probed using the charge transfer resistance (R_{ct}) in the high frequency region, where R_{ct} shows a dependence on lithium insertion and extraction rates. This analysis shows that $LiMn_{0.95}Ni_{0.05}PO_4/C$ has the lowest R_{ct} value, indicating that the Li^+ ions are inserted and extracted in this material faster than others. In general, all the Nyquist plots in Fig. 5 show that Ni doping can improve the Li^+ kinetics by reducing cell impedance. These results suggest that cycling measurements should be performed to determine the effect of Ni doping on the stability over many cycles. Fig. 6 shows the charge-discharge curves in the first cycle for the cells made using the samples. The Ni doped samples have much higher discharge capacities. From $x = 0$ to 0.1, the cells show initial discharge capacities of 93.5, 104.7, 118.5, 127.4 and 114.9 $mAh \cdot g^{-1}$. In this testing, $LiMn_{0.95}Ni_{0.05}PO_4/C$ again has the best electrochemical performance. Specific capacity measurements during cycling, shown in Fig. 7, demonstrate that the superior performance of $LiMn_{0.95}Ni_{0.05}PO_4/C$ is maintained over 50 cycles. From Fig. 7, it is seen that the Ni-doped samples show better cycling performance. After 50 cycles, the specific capacity of $LiMn_{0.95}Ni_{0.05}PO_4/C$ retained 88.9 % of its initial value, while the undoped $LiMnPO_4/C$ retained 82.2 % of its initial capacity. It was found that the initial and specific capacity after 50 cycles were correlated and all the samples retained between 88.9 % and 82.2 % of their initial capacity. A summary of the initial discharge capacity, and discharge capacity after 50 cycles for all the samples is shown in Fig. 8. From the above analysis, the superior performance of Ni-doped $LiMnPO_4/C$ samples can be attributed to the following effects of Ni doping: 1) enhancement of the bulk electronic conductivity, 2) reduction of particle aggregation, 3) increase in the Li^+ diffusion speed, 4) reduction in R_{ct}.

4. Conclusions

Ni doped $LiMnPO_4/C$ was synthesized using spray-drying followed by ball milling. All the samples consisted of a single olivine phase. The results show that Ni doping can increase the bulk electronic conductivity of $LiMnPO_4$, reduce its resistance to lithium ion charge transfer, and inhibit particle aggregation. Together, these factors can significantly improve the electrochemical per-

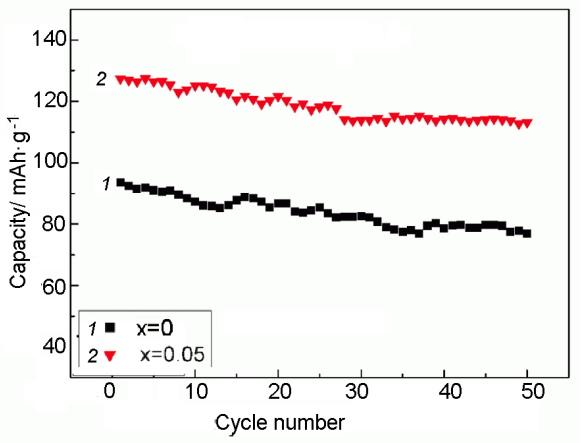

Fig. 7. Cycling performance of $LiMn_{1-x}Ni_xPO_4/C$.

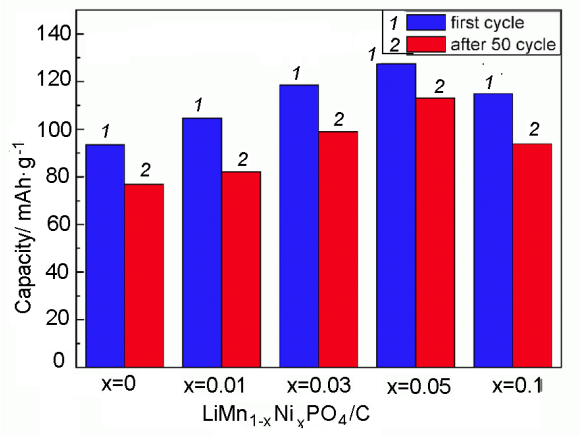

Fig. 8. Comparison of the discharge capacity of the fully charged electrodes, during the first cycle and after 50 cycles.

formance of $LiMnPO_4$. Therefore, an appropriate level of Ni doping was shown to be a useful method to overcome the existing problems of $LiMnPO_4$ cathodes for high power applications.

Acknowledgement. This study was supported by the National Basic Research Program of China (973 Program, 2014CB643406), and the National Key Technology Support Program (2015BAB06B00).

References

1. L.Wu, S.K.Zhong, *Ionics*, **19**, 1061 (2013).
2. Luo, J.R.Dahn, *Electroch.Acta*, **54**, 4655 (2009).
3. Z.Yang, G.S.Cao, *Solid State Electrochem.*, **1271**, (2012).
4. T.N.L.Doan, Z.Bakenov, *Adv.Powder Techn.*, **21**, 187 (2010).
5. Y.Mizuno, M.Kotobuki, ????, **117**, 1225 (2009).
6. Yan Bofeng, Zeng Ming, *Functional Materials*, **26**, 205 (2019).
7. P.Yan, L.Lu, X.Liu, *Mater.Chem.A*, **1**, 10429 (2013).
8. X.L.Pan, C.Y.Xu, *Electrochim.Acta*, **87**, 303 (2013).
9. V.Kolea, D.Stoilova, *J. Solid State Chem.*, **133(2)**, 416 (1997).
10. K.Wang, R.Cai, *Electrochim.Acta*, **54**, 2861 (2009).
11. S.Moon, D.K.Kim, *Ceram.Int.*, **38**, 471 (2012).
12. F.X.Wu, X.H,Li, *Power Sour.*, **202**, 374 (2012)
13. J.Z.Li, S.H.Luo, *J.Electrochem.Soc.*, **166**, A118 (2019).
14. H.Yang, J.Y.Liu, *Nanofibers.Chem.Sus.Chem.*, **12**, 3817 (2019).
15. R.Veena, P.Puspamitra, *Surface Scien.*, **495**, 143541 (2019).
16. R.El Khalfaouy, A.Addaou, *Alloys Compd.*, 775 (2019).
17. J.Li, S.Luo, *Appl.Mater.Interfaces*, **10**, 10786 (2018).